OCEANOGRAPHY

Caribbean salinity anomalies contributed to variable North Atlantic circulation and climate during the Common Era

Anastasia Zhuravleva[1,2]*, Henning A. Bauch[2,3]*, Mahyar Mohtadi[4], Kirsten Fahl[3], Markus Kienast[1]

Paleoceanographic reconstructions show that the strength of North Atlantic currents decreased during the Little Ice Age. In contrast, the role of ocean circulation in climate regulation during earlier historical epochs of the Common Era (C.E.) remains unclear. Here, we reconstruct sea surface temperature (SST) and salinity in the Caribbean Basin for the past 1700 years using the isotopic and elemental composition of planktic foraminifera tests. Centennial-scale SST and salinity variations in the Caribbean co-occur with (hydro)climate changes in the Northern Hemisphere and are linked to a North Atlantic SST forcing. Cold phases around 600, 800, and 1400 to 1600 C.E. are characterized by Caribbean salinification and Gulf of Mexico freshening that implies reductions in the strength of North Atlantic surface circulation. We suggest that the associated changes in the meridional salt advection contributed to the historical climate variability of the C.E.

INTRODUCTION

The Common Era (C.E.; past 2000 years) is a key time interval for understanding climate responses to both natural and anthropogenic forcing mechanisms and for testing the performance of model simulations (*1*). This period is associated with several climate epochs, such as the Late Antique Little Ice Age [536 to 660 C.E., (*2*)], the Medieval Warm Period [950 to 1250 C.E., (*3*)], the Little Ice Age [LIA; ca. 1400 to 1850 C.E., (*3*, *4*)], and the 20th-century warming (*5*).

For the LIA, the prevailing paradigm suggests that the initial transient cooling of the North Atlantic was caused by external forcing, such as enhanced volcanism combined with weak solar activity (*6*, *7*, *8*). However, it is also argued that internal climate feedbacks associated with the expansion of Arctic sea ice were essential in maintaining cold sea surface temperatures (SSTs) over centennial timescales (*9*). According to this scenario, the volcanically triggered excess of sea ice was exported into the Labrador Sea, where its melting caused reductions in the strength of the subpolar gyre, deep-water formation, and possibly the Atlantic Meridional Overturning Circulation (*10*). Consequently, the northward transport of warm and saline tropical waters from the Gulf Stream declined (*11*–*14*), which reinforced cooling and sea ice expansion in the subpolar North Atlantic and led to the onset of the coldest LIA conditions (*15*). While geochemical and sedimentological proxy data confirm a weakened ocean circulation during the LIA [see, e.g., (*6*)], there is little information on earlier epochs of the C.E. An accurate representation of past variability in circulation is, however, essential to better constrain the role of internal ocean dynamics in climate regulation and to test climate models.

Thirumalai *et al.* (*14*) suggested that sea surface salinity (SSS) changes in the Atlantic Ocean can be used as a diagnostic parameter of surface circulation. In particular, salinification of the southeastern Caribbean and freshening of the Gulf of Mexico and subpolar North Atlantic have been linked with a weakening of surface currents and a reduction of meridional salt advection on multidecadal timescales (*14*). Thirumalai *et al.* (*14*) further reconstructed a pronounced centennial-scale SSS variability in the northern Gulf of Mexico during the C.E. and linked these changes to variable northward transport of saline tropical water via the Loop Current, which is a mixed-layer current upstream of the Gulf Stream (Fig. 1A).

In light of these findings, reconstruction of SSS variability in the southeastern Caribbean during the C.E. can help to assess whether the same processes/feedbacks as discussed for multidecadal timescales in (*14*) (e.g., weaker surface currents and salinity build-up in the tropics) were at play on centennial timescales as well. However, direct evidence of salinity changes in the tropical western North Atlantic during the C.E. is missing so far, primarily due to the lack of suitable reconstructions [but see (*16*)]. For example, existing proxy records from the Caribbean based on corals and sclerosponges do not fully cover the transition between the Medieval Warm Period and the LIA (*17*, *18*), whereas sediment records from the Cariaco Basin, off the coast of Venezuela, can be overprinted by seasonal upwelling (*19*).

To constrain ocean circulation changes during the C.E. in the context of the hypothesis of Thirumalai *et al.* (*14*), we reconstructed SST and SSS for the past ~1700 years from a box core profile retrieved from the Tobago Basin in the southeastern Caribbean (M35003-6, 12°5.1′N, 61°14.7′W, blue circle with red border in Fig. 1B). The high sedimentation rates in this area [see, e.g., (*20*)], a result of continuous influx of suspended sediment load from the Orinoco and Amazon Rivers, allowed for ~30- to 100-year sampling resolution , which is perfect for studying centennial SST/SSS variability (see Supplementary Text). We observe a negative relationship between SSS in the southeastern Caribbean and the Gulf of Mexico on centennial timescales, likely indicative of variations in the strength of the North Atlantic surface circulation. We posit that the associated changes in the northward advection of (sub)tropical salt influenced ocean circulation and climate of the C.E.

[1]Department of Oceanography, Dalhousie University, Halifax, NS, Canada. [2]GEOMAR Helmholtz Centre for Ocean Research, Kiel, Germany. [3]Alfred Wegener Institute Helmholtz Centre for Polar and Marine Research, Bremerhaven, Germany. [4]MARUM - Center for Marine Environmental Sciences, University of Bremen, Bremen, Germany.
*Corresponding author. Email: anastasia.zhuravleva@dal.ca (A.Z.); hbauch@geomar.de (H.A.B.)

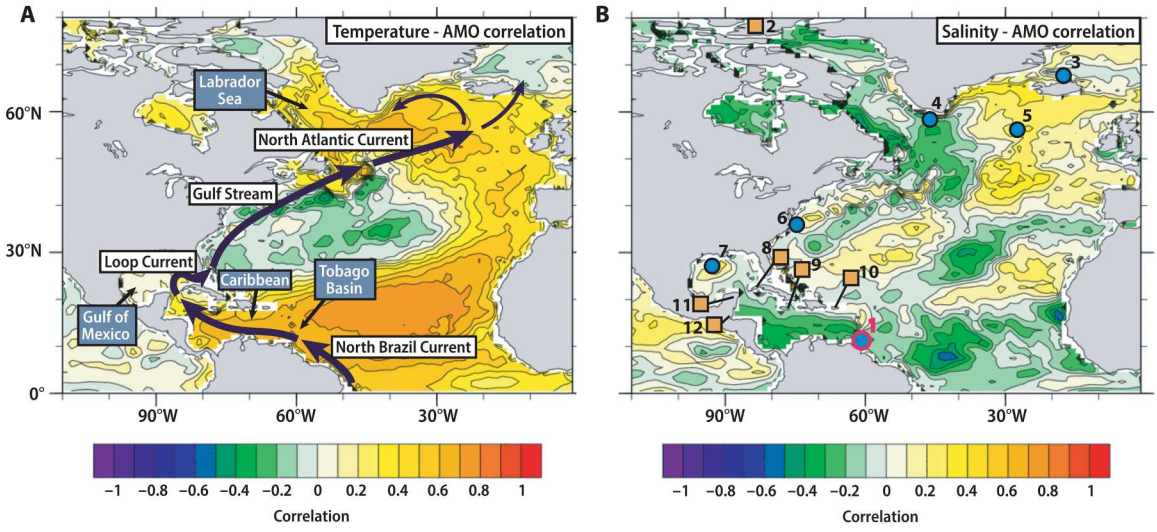

Fig. 1. Correlation between the AMO and North Atlantic surface water properties and the locations of proxy records. Correlation maps are created in the Web-based Reanalyses Intercomparison Tools (https://psl.noaa.gov/data/writ/) using temperature (**A**) and salinity (**B**) data at 20-m water depth from ORA-S5 dataset [from 1979 to 2022, (*58*)] and a detrended AMO index from NOAA website (www.psl.noaa.gov/data/timeseries/AMO/). The numbering 1 to 12 in (B) corresponds to sites referred to in the text (see table S1 for details): (1) M35003-6, Tobago Basin, southeastern Caribbean (this study), (2) South Sawtooth Lake, Canada (*15*), (3) *Arctica islandica* site, North Icelandic shelf, Nordic Seas (*12*, *13*), (4) RAPiD-35-COM, Labrador Sea (*10*), (5) RAPiD-21-COM, subpolar Northeastern Atlantic (*10*), (6) KNR-178-48JPC, western North Atlantic (*47*), (7) 2010-GB2-MCA, Gulf of Mexico (*14*), (8) CG stalagmite, Cuba (*38*), (9) PDR-1 stalagmite, Puerto-Rico (*37*), (10) Grape Tree Pond, Jamaica (*36*), (11) Lake Punta Laguna, Yucatan, Mexico (*33*), (12) YOK-I stalagmite, Yucatan, Belize (*35*). Marine and terrestrial-based proxy locations are marked with circles and squares, respectively. AMO, Atlantic Multidecadal Oscillation.

RESULTS

Foraminiferal SST/SSS and uncertainties

We measured magnesium-to-calcium (Mg/Ca) and stable oxygen isotope ratios ($\delta^{18}O$) in planktic foraminifera *Globigerinoides ruber* (white) to reconstruct upper ocean temperatures and salinities (here referred to as SST and SSS) in the Tobago Basin, southeastern Caribbean (Fig. 2 and fig. S1). Our SST estimate for the core top is 1.3 ± 0.5°C lower than previously obtained at this site (see Supplementary Text). While absolute SST/SSS estimates have only marginal effects on the discussed downcore anomalies, the agreement between our core-top estimates of SST (26.7 ± 0.3°C) and SSS (35.6 ± 0.2 U) and the observed annual climatology (Fig. 3) suggests that *G. ruber* (white) tests can be used to reconstruct the annual signal. We note, however, that until detailed sediment traps become available for the Tobago Basin (*21*, *22*), it cannot be resolved whether a seasonal bias in planktic foraminifera fluxes and geochemical proxies exists at our location (see Materials and Methods). Nevertheless, this caveat has little impact on our interpretation because we rely on the covariate variability in several proxy datasets with potential seasonal biases.

Centennial-scale climate variability in the southeastern Caribbean

SST, SSS, and associated uncertainties were calculated from paired Mg/Ca-$\delta^{18}O$ values in PSU Solver (*23*), a MATLAB code that uses a bootstrap Monte Carlo framework (see Materials and Methods). The average 1σ (2σ) uncertainties are about ±0.5°C (0.8°C) for SST and ±0.3 U (0.6) for SSS. Considering that C.E. temperature anomalies (51-year low-pass–filtered global data) often do not exceed ±0.5°C (*5*) and that bioturbation can additionally dampen the downcore climate signal, we interpret our SST/SSS records within a 1σ error. Because of the unavoidably high dating uncertainty of our Caribbean core, the age model was based on alignment to the well-dated Gulf of Mexico core 2010-GB2-MCA (*14*) (see Supplementary Text). We interpret smoothed by three-point moving average records that allow us to examine centennial climate variability without over-smoothing the intervals with low temporal resolution, such as the LIA (~100 years/cm; fig. S2).

The $\delta^{18}O$ record of *G. ruber* (white), which contains both SST and SSS signals, reveals pronounced centennial variability during the first millennium of the C.E. (Fig. 2A). Two intervals at ~550 to 650 C.E. and ~750 to 900 C.E. show average $\delta^{18}O$ values higher by 0.4 ± 0.1‰ compared to immediately adjacent data points, clearly indicating episodes of salinification and/or cooling in the southeastern Caribbean. Colder SST at ca. 850 C.E. (1.5 ± 0.7°C lower than adjacent values) is corroborated by PSU Solver estimations (Fig. 2B), and both high-$\delta^{18}O$ intervals are associated with higher salinity by 0.6 ± 0.4 U relative to the adjacent samples (Fig. 2C). Although the interval with high $\delta^{18}O$ values at ~750 to 900 C.E. is characterized by substantial SSS variability, the positive salinity anomaly at 800 C.E. is unambiguously represented by three consecutive data points. BEAST, a Bayesian change point detection algorithm (*24*), supports the inferred SSS changes and the overall identification of the climate intervals (see Materials and Methods). We note that the probability of a change point indicating the onset of the salinification event around 550 C.E. decreases sharply when the high SSS value around 630 C.E. (35.8 ± 0.2 U) is removed from the raw dataset (Fig. 2C). However, this value was not derived from outliers (see Materials and Methods), and even its removal does not affect our interpretation, as several consecutive data points indicate the subsequent freshening around 700 C.E. Thus, we conclude that, despite pronounced variability and

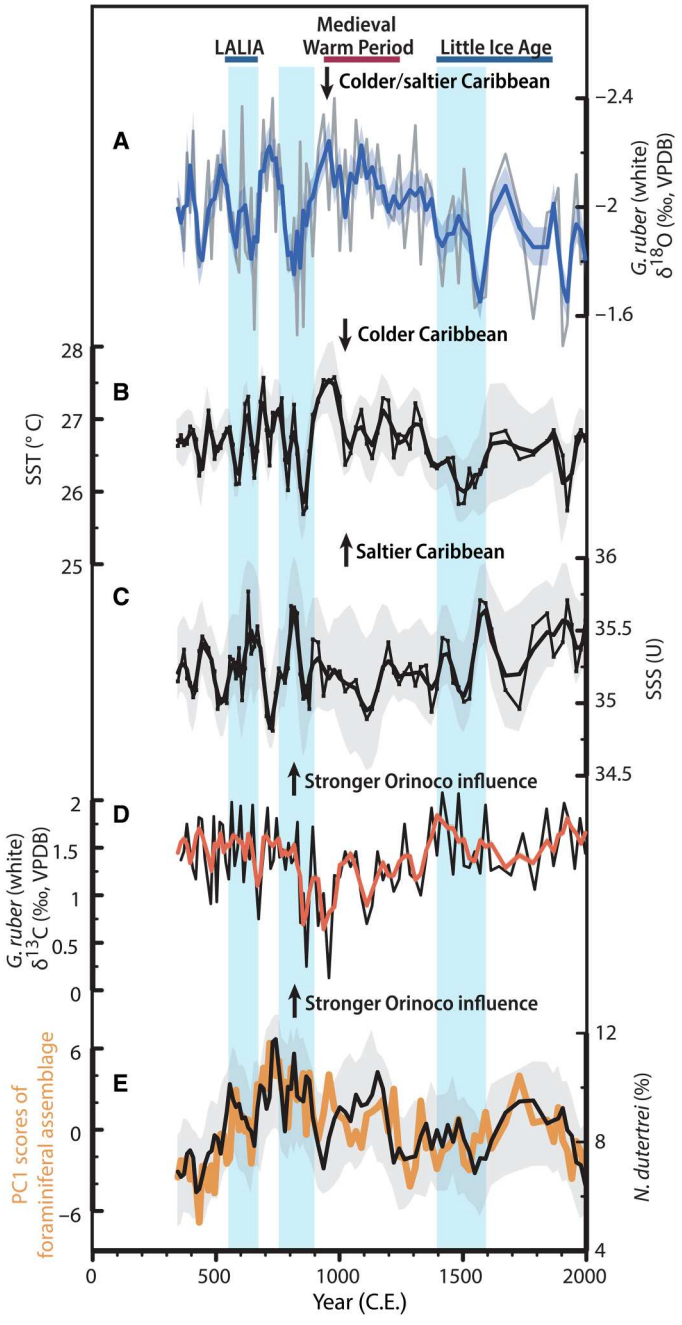

Fig. 2. Climate proxy records from core M350036 over the past 1700 years. (**A**) Planktic $\delta^{18}O$ values, (**B**) SST, (**C**) SSS, (**D**) planktic $\delta^{13}C$ values, and (**E**) proportions of *N. dutertrei* (black, 3-point moving average smoothed record) and scores for the first principal component (PC1) of planktic foraminifera assemblage (orange, raw data). In (A) to (D), both raw and smoothed (3-point moving average) data are shown. Smoothed records are plotted with their ±1σ uncertainties (A to D) and 95% confidence intervals for *N. dutertrei* proportions (E). Blue bars denote centennial cooling/salinification events in the southeastern Caribbean. LALIA, Late Antique Little Ice Age.

some uncertainties, our data reveal two intervals of higher SSS during the first millennium of the C.E.

For the LIA interval between ca. 1400 and 1600 C.E. referred here to as the "early LIA peak", we find high $\delta^{18}O$ values (~0.4 ± 0.1‰ higher than the adjacent), which imply cold and/or salty conditions. PSU Solver suggests for this time interval ~0.9 ± 0.6°C colder SST than for the core top. PSU Solver and BEAST further reveal an increase in salinity by 0.7 ± 0.4 U at ca. 1550 C.E. This salinification signal is found at the end of the early LIA peak cooling; however, a small-scale SSS increase is also detected around 1450 C.E. The later part of the LIA (ca. 1600 to 1850 C.E.) is characterized by relatively warm SST, highly variable $\delta^{18}O$ and SSS, e.g., fresh conditions around 1700 C.E. and high salinities at 1850 C.E. Because of the low resolution and thus high chronological uncertainties of this later LIA period (fig. S2), we limit our interpretation to the early LIA peak (1400 to 1600 C.E.), associated with relatively cold and salty conditions in the southeastern Caribbean.

Evidence of low Orinoco influence on downcore SSS changes

Because of its proximity, the influence of the Orinoco River on reconstructed SSS at our site must be addressed. On the one hand, the increased influence of Orinoco freshwater can result in lower SSS by reducing $\delta^{18}O$ values in foraminiferal calcite. On the other, increased Orinoco outflow can bias our proxy records to higher SSS because of the low pH of river water [5.5 to 7.5, (*25*)] that can increase Mg/Ca values. If there was a notable impact, then we would expect SSS estimates to covary to some extent with foraminiferal carbon isotope composition ($\delta^{13}C$), a proxy for mixed-layer productivity controlled at our location by riverine nutrients (*26*, *27*). Although a coeval reduction in SSS and $\delta^{13}C$ values is observed at 850 C.E. (Fig. 2, C and D), the overall correlation for the raw data is insignificant ($r = 0.19$, $P > 0.05$), and visual assessment further suggests that other SSS changes are not related to $\delta^{13}C$ shifts. Planktic foraminifera assemblage data can also help separate the Orinoco influence because the latter controls primary productivity and turbidity in the southern Tobago Basin (*21*, *22*, *27*). Again, if reconstructed SSS relates to the Orinoco freshwater, then we expect it to covary with the assemblage data. Our principal components analysis (PCA) on the assemblage dataset shows no correlation between SSS and the three significant principal components (PCs; figs. S3 to S5). In addition, there is no correlation between reconstructed SSS and the proportional abundances of *Neogloboquadrina dutertrei* ($r = -0.12$, $P > 0.05$, raw data). This species defines the scores for the first PC (Fig. 2E) and is characteristic of elevated Orinoco-derived nutrient concentrations (*22*). While planktic $\delta^{13}C$ and assemblage data do not agree with each other (possibly due to dependence on additional non-Orinoco factors), the overall lack of covariation with the inferred SSS changes suggests that the latter are not strongly affected by the Orinoco runoff. This is supported by Caribbean data indicating that Orinoco freshwater does not overprint foraminiferal $\delta^{18}O$ values because they are predominantly affected by the evaporation minus precipitation (E − P) signal (*21*). Accordingly, we interpret the reconstructed SSS signal to be primarily controlled by ocean-atmosphere processes (*28*, *29*).

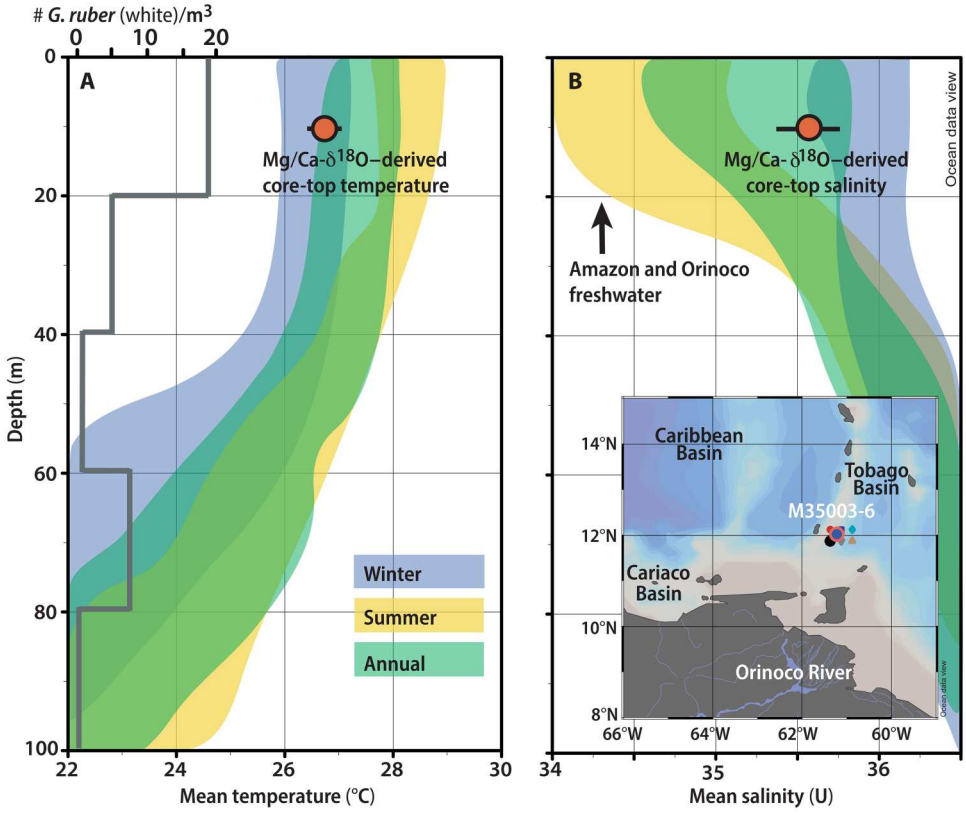

Fig. 3. Modern climatology in the southern Tobago Basin and reconstructed temperature/salinity for the M35003-6 core top. Mean annual and seasonal temperature (**A**) and salinity (**B**) in the upper 100 m for the past six decades approximated from six nearest to M35003-6 stations in the World Ocean Atlas (*59*) [see the inset map in (B)]. Orange circles with bars show temperature and salinity estimates (±1σ) for the M35003-6 core top derived from Mg/Ca-δ^{18}O values. Also shown in (A) is the depth distribution of living *G. ruber* (white) in the fraction of >100 μm inferred from multiple opening/closing plankton nets at our core location in April 1996 (*22*). The figure is made using Ocean Data View (*60*).

DISCUSSION

Caribbean cooling/salinification and regional hydroclimate

Instrumental data, models, and paleo studies indicate that precipitation amounts in the circum-Caribbean region and Americas are tied to tropical Atlantic temperatures (*28*, *30*, *31*). Colder (warmer) SSTs in the tropical North Atlantic are linked with a smaller (larger) Atlantic Warm Pool, which is a body of warm water (>28.5°C) that appears in the Caribbean Basin, the Gulf of Mexico, and the western tropical North Atlantic during the summer/fall season (*30*). The Atlantic Warm Pool enhances moisture convergence across the Caribbean by weakening the North Atlantic Subtropical High and enhancing precipitable water across the Intertropical Convergence Zone (*28*, *30*). Therefore, a small Atlantic Warm Pool can induce an anomalous descent flow and generate less precipitation in the region (*28*, *32*). In addition, Caribbean cooling favors an increased pressure gradient between the Atlantic and Pacific basins, leading to a stronger atmospheric moisture export across Central America and thus less precipitation in the circum-Caribbean land (*28*). In light of this coupling, a comparison of our Caribbean SST/SSS with regional precipitation records is presented to support our reconstruction.

During the first millennium of the C.E., our records reveal a pronounced cooling/salinification in the Caribbean at ca. 750 to 900 C.E. (Fig. 4A). This event can be associated with the severe droughts in the Yucatan Peninsula (Fig. 4, D and E) that likely coincided with the disintegration of the Classic Mayan civilization between 800 and 950 C.E. (*33*–*35*). Despite the considerable spatiotemporal complexity of precipitation variability in the region, a recent data synthesis confirmed drought coherence in Mesoamerica between 800 and 1050 C.E. and tentatively linked it with the cooling of tropical Atlantic SST (*31*). Such cooling had not, however, been indicated by Caribbean SST/SSS records, possibly due to their lower temporal resolution or methodological uncertainties (*16*, *19*). In contrast, low SST around this time is revealed in our Caribbean record and is supported by reconstructions from the Gulf of Mexico (Fig. 4A) (*14*). We further hypothesize that the positive Caribbean SSS anomaly at ca. 550 to 650 C.E. corresponds to the Late Antique LIA between 536 and 660 C.E. (*2*). This widespread Northern Hemisphere cooling was marked by crop failures, famines, and societal changes in Europe and Asia (*2*). Bayesian analysis of the timing of dry intervals, performed with the three lacustrine records from southern Mexico (*31*), including, for example, δ^{18}O record from Punta Laguna (Fig. 4D), suggests a higher-than-noise probability for drought between 400 and 600 C.E. However, drier conditions around this time are not supported by other reconstructions (Fig. 4E) (*35*).

For the LIA interval, x-ray fluorescence data from the Grape Tree Pond (Jamaica) suggest lowered precipitation amounts in the northwestern Caribbean between ca. 1400 and 1600 C.E. (Fig. 4C) (*36*), in

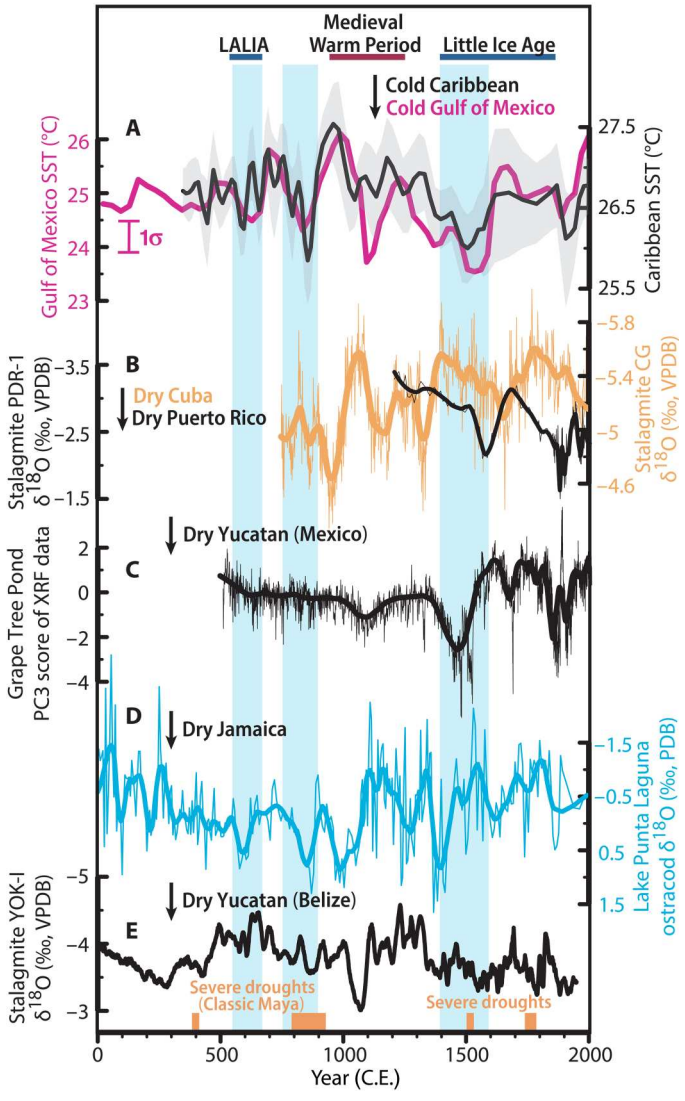

Fig. 4. Proxy records of hydroclimate in the low-latitude North Atlantic and circum-Caribbean land during the past 2000 years. (**A**) SST records from the Caribbean core M35003-6 (black, this study) and Gulf of Mexico core 2010-GB2-MCA [magenta, (*14*)]. Smoothed records are shown and interpreted (for M35003-6, three-point moving average; for 2010-GB2-MCA, 2σ age model uncertainty; see Supplementary Text). (**B**) $\delta^{18}O$ signal (original and 10% loess-filtered records) of stalagmites CG, Cuba [orange, (*38*)] and PDR-1, Puerto Rico [black, (*37*)]. (**C**) The third principal component (PC3) of x-ray fluorescence (XRF) data from core GT-3, Grape Tree Pond, Jamaica [original and 10% loess-filtered records, (*36*)]. (**D**) Ostracod *Cytheridella ilosvayi* $\delta^{18}O$ values (original and 2% loess-filtered records) in the sediment core from Lake Punta Laguna, southern Mexico (*33*). (**E**) $\delta^{18}O$ of stalagmite YOK-I, Belize (*35*). Orange bars show major droughts during the Classic Maya civilization (300 to 1000 C.E.) based on (*34*, and two historic droughts in the Yucatan in the 16th and 18th century C.E. (*35*). For locations of sites, refer to Fig. 1B and table S1. Blue bars denote centennial cooling/salinification events in the southeastern Caribbean.

agreement with the early LIA peak cooling in our record (Fig. 4A). The low $\delta^{18}O$ values in a Puerto-Rican stalagmite indicate drier conditions in the northern Caribbean around 1600 C.E. (Fig. 4B) (*37*), while a Cuban stalagmite record shows a drying trend that culminates at ca. 1650 C.E. (Fig. 4B) (*38*). Pronounced drying events between 1350 and 1650 C.E. are also evident in the Yucatan Peninsula from elevated $\delta^{18}O$ values in the lacustrine record from Punta Laguna (Fig. 4D) (*33*) and positive $\delta^{18}O$ anomalies in the Belize stalagmite record (Fig 4E) (*35*). In contrast to these dry episodes during the early LIA, precipitation amounts in the Yucatan Peninsula and Caribbean islands were generally increased during the later LIA phase (1600–1850 C.E.). The climate evolution recorded by these records contrasts with the uniformly dry conditions in northern South America during the entire duration of the LIA (1450 to 1850 C.E.), as indicated by the low titanium percent in the Cariaco sediment record (*39*), but is more consistent with the cold/warm LIA phases observed in our Caribbean SST record, as well as in the Gulf of Mexico reconstruction (Fig. 4A).

The visual assessment suggests a broad agreement between intervals of the Caribbean cooling/salinification and drying in the circum-Caribbean land, reaffirming that our SST and SSS reconstructions are not subject to the strong influence of local climate variables (e.g., discharge from the Orinoco River). Furthermore, this comparison underscores the dominant role of the tropical Atlantic in controlling centennial-scale rainfall changes in the region (*30*). However, inconsistencies between the tropical SST and hydroclimate records highlight the spatiotemporal complexity in regional precipitation variability, which is likely due to a large number of forcing factors, such as the coupled Atlantic-Pacific ocean-atmosphere dynamics, and topography.

A mechanism for tropical salinification

Annual SST in the tropical North Atlantic correlates with the Atlantic Multidecadal Oscillation (AMO) indexes (Fig. 1A). The traditional AMO index is often defined as a 10-year running mean of linearly detrended annual SST anomalies averaged over the entire North Atlantic, as first proposed by Enfield *et al.* (*40*). Positive AMO phases expressed as anomalously high SST in the North Atlantic are associated with tropical warming while cooling in the low latitudes occurs during negative AMO phases (*40*). In addition, long-term observational SSS datasets from across the Atlantic suggest a negative correlation between the AMO and northern tropical SSS (Fig. 1B). In particular, positive AMO phases are related to tropical North Atlantic freshening, while negative AMO indexes are linked with salinification in the low latitudes (*41*). The tropical SSS responds to the North Atlantic SST changes via latitudinal displacements of the Intertropical Convergence Zone and the Atlantic Warm Pool variations through their effects on the E − P patterns and moisture transport across Central America [see above and (*28*, *32*, *42*)]. In the western (sub)tropical North Atlantic, negative phases of the AMO are further linked with reduced transport of northerly directed surface currents, such as the North Brazil Current and the Loop Current (Fig. 1A) (*43*, *44*).

A lacustrine record from the Canadian Arctic is considered a reliable proxy for the past AMO as it correlates with SST over the subpolar North Atlantic (Fig. 5A) (*15*). Prolonged periods of negative mean states of the AMO in this record (i.e., cold SST in the subpolar North Atlantic) around 600, 800, and 1400 to 1600 C.E. visually agree with the timing of inferred cooling/salinification events in

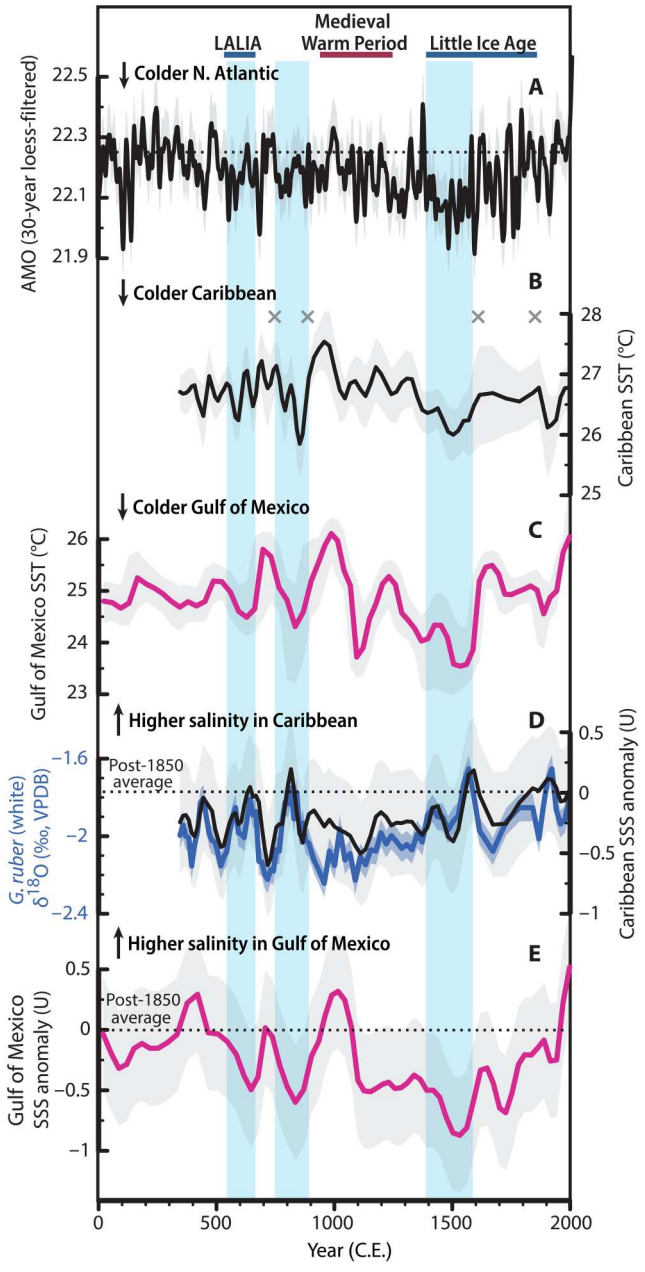

Fig. 5. Relation between SST/SSS in the North Atlantic, southeastern Caribbean, and the Gulf of Mexico during the past 2000 years. (**A**) Thirty-year loess-filtered record of reconstructed AMO [±2σ, (*15*)]. (**B** and **C**) SST and (**D** and **E**) SSS anomalies with respect to the modern era (post-1850 C.E.) reconstructed from Caribbean core M35003-6 (black, this study) and Gulf of Mexico core 2010-GB2-MCA [magenta, (*14*)] with their ±1σ uncertainties. Also shown in (D) is the foraminiferal $\delta^{18}O$ record for core M35003-6 (blue, ±1σ). Smoothed records are shown and interpreted (for M35003-6, three-point moving average; for 2010-GB2-MCA, 2σ age model uncertainty; see Supplementary Text). The dashed horizontal line in (A) is the estimated average value over the past 1850 years. Gray crosses indicate tie points used for age model construction (see Supplementary Text). Blue bars indicate intervals of cooling/salinification in the southeastern Caribbean.

the Caribbean (Fig. 5D). Accordingly, correlation statistics shows that the estimated Caribbean and Gulf of Mexico SSTs (i.e., reference core 2010-GB2-MCA; see Supplementary Text) (Fig. 5, B and C) correlate with the aforementioned AMO reconstruction (r = 0.30, $P < 0.01$ for Caribbean; r = 0.47, $P < 0.01$ for Gulf of Mexico). Implying similar ocean-atmosphere processes on multidecadal and centennial timescales [see, e.g., (*31*)], we suggest that the C.E. cooling/salinification events developed in the southeastern Caribbean in response to subpolar North Atlantic colder SST that caused southward shifts of the Intertropical Convergence Zone, smaller Atlantic Warm Pool sizes and, therefore, reduced precipitation in the Caribbean region coupled with increased moisture export to the Pacific. Changes in the ocean circulation likely amplified SSS changes in the Caribbean (see below).

Comparison of Caribbean and Gulf of Mexico paleosalinity records

Comparison of SSS anomalies (relative to the modern era, post-1850 C.E.) reconstructed for the Caribbean (this study) and the Gulf of Mexico (*14*) reveals a negative relationship between 550 and 1050 C.E. (Fig. 5, D and E). While SST records correlate at no phase lag (r = 0.61, $P < 0.01$), the SSS records are antiphased (r = −0.56, $P < 0.01$). On the basis of our reconstruction, two salinification events in the Caribbean centered at ca. 600 and 800 C.E. correspond to freshening and cooling in the Gulf of Mexico, whereas warmer conditions at ca. 700 C.E. and the medieval peak warmth at ca. 1000 C.E. are associated with fresher Caribbean but saltier Gulf of Mexico. We note that although the two SST records were aligned (see Supplementary Text), the SSS seesaw over this time interval partially remains even if the age model for our core is built exclusively on radiocarbon dates (fig. S6).

For the LIA, statistical analysis does not reveal significant cross-correlation between the SSS records on the current timescales. The low temporal resolution and limited chronological constraints during this time interval can hinder the precise assessment of the SSS phasing during the LIA. Nevertheless, we note that particularly fresh and cold surface conditions have been reconstructed in the Gulf of Mexico during the early LIA peak cooling, i.e., between 1400 and 1600 C.E., while subsequent warmer phase is associated with increased SSS (Fig. 5E). In contrast, the early LIA peak cooling in the Caribbean contains a pronounced salinity anomaly (1500 to 1600 C.E.) and a small SSS increase at 1400 C.E., while the onset of the warmer spell at 1600 C.E. is characterized by an abrupt reduction in SSS and $\delta^{18}O$ values in planktic foraminifera (Fig. 5D). This observation suggests a possibility for an antiphase behavior, in agreement with the conditions between 550 and 1050 C.E.

Overall, our data suggest a negative correlation between the SSS in the Caribbean and the Gulf of Mexico on centennial timescales. However, future work is needed to more robustly (statistically) confirm the SSS seesaw, especially during the LIA, and to identify potential phase lags.

The SSS seesaw between the Caribbean and the Gulf of Mexico is evident on multidecadal timescales from observation-based data (Fig. 1B). However, the antiphase behavior was not confirmed for the centennial timescales: While no proxy data existed, a weak but positive correlation between SSSs was revealed by the Max Plank Institute Earth System Model for paleo-applications (MPI-ESM-P) using a 50- to 150-year bandpass filter (*14*). In contrast, our

study suggests that the Caribbean–Gulf of Mexico SSS seesaw holds also on centennial timescales. This finding implies that the forcing mechanisms responsible for the SSS changes (i.e., coupled ocean-atmosphere processes; see below) could be at play on higher frequencies in the model or that the model simulation of centennial SSS patterns is biased.

Mechanisms for the Caribbean–Gulf of Mexico salinity seesaw

To explain the concomitant freshening in the northern Gulf of Mexico and salinification in the southeastern Caribbean on centennial timescales, atmospheric circulation dynamics linked with the North Atlantic SST anomalies can be invoked. Colder North Atlantic SST is associated with annual E − P anomalies that are negative in the Gulf of Mexico but positive in the southeastern Caribbean, leading to the opposite trends in surface salinity (*28*, *32*, *42*). The associated southward shift of the Intertropical Convergence Zone, intensification of the north-eastern trade winds, and, to a lesser extent, of the Atlantic Warm Pool, can additionally hinder the intrusion of the warm and salty tropical waters into the northern Gulf of Mexico leading to colder and fresher conditions in the region (*45*).

Critically, we argue that oceanic circulation acted in synergy with the atmospheric processes to generate the SSS seesaw. Thirumalai *et al*. (*14*) suggested that simultaneous freshening and cooling of the northern Gulf of Mexico is associated with the weakening of the North Atlantic surface currents on multidecadal-to-centennial timescales. This involves reductions in the strength of the Loop Current (downstream of the North Brazil Current and upstream of the Gulf Stream; Fig. 1A), transporting warm and salty Caribbean water into the Gulf of Mexico (*44*, *45*). Therefore, simultaneous reductions in the Gulf of Mexico SST and SSS at ca. 600, 800, and 1400 to 1600 C.E. (Fig. 5, C and E) might indicate a weakening of the North Atlantic surface currents, e.g., the Loop Current and the North Brazil Current. These time intervals appear coeval with the Caribbean salinification (Fig. 5D).

Our Caribbean data alone cannot establish that water mass advection is a major control on negative SSS correlation between the Caribbean and the Gulf of Mexico (*14*), but they are consistent with this hypothesis. In particular, a reduced strength of the North Brazil Current and thus lowered advection of low-salinity water from the Amazon River could increase SSS in the Caribbean. This advective process dominates the salinity cycle in the western tropical Atlantic on annual timescales (*29*).

To more directly establish that ocean circulation was an important driver of concomitant salinity changes in the Caribbean and the Gulf of Mexico on centennial timescales, we calculated the difference between reconstructed SSS anomalies in these regions (ΔSSS; Fig. 6A). To the extent that this gradient relates to meridional salt transport via changing North Atlantic currents, we expect it to covary with proxy reconstructions of ocean circulation. In agreement with our ΔSSS record, pronounced reductions in the Gulf Stream and the North Atlantic Current have been demonstrated for the LIA (Fig. 6B) (*11*–*14*). Robust evidence for variations in the strength of the North Atlantic currents beyond the LIA is scarce, however, a decline in the Atlantic-derived waters has been documented in the southern Nordic Seas around 800 C.E. (Fig. 6B) (*12*). This change in ocean circulation corresponds to Caribbean salinification and Gulf of Mexico freshening (i.e., low ΔSSS) supporting our concept.

Variations in the large-scale North Atlantic surface circulation can arise from changes in the strength of the subpolar gyre and the Labrador Sea Water formation (*10*, *46*). To assess changes in the Labrador Sea convection during the C.E., we used two records from the North Atlantic, one from the western North Atlantic (core KNR-178-48JPC), which directly approximates the flow speed of the southward-flowing Labrador Sea Water within the Deep Western Boundary Current (Fig. 6D) (*47*). The other record, from the Gardar Drift in the subpolar eastern North Atlantic (core RAPiD-21-COM), provides indirect evidence of changes in the Labrador Sea convection through its interaction with the Iceland-Scotland Overflow Water: Faster Iceland-Scotland Overflow Water flow velocities during cold climate anomalies are, thus, interpreted as resulting from a reduction in Labrador Sea Water formation (Fig. 6C) (*10*). A visual comparison of proxy records suggests that periods of reduced convection in the Labrador Sea (Fig. 6, C and D) correspond with intervals of lowered ΔSSS (Fig. 6A). Within the uncertainties of the age models, these changes are also consistent with a weaker subpolar gyre (Fig. 6E) (*10*). This proxy data agreement supports the critical role of ocean circulation in developing the SSS seesaw between the southeastern Caribbean Basin and the Gulf of Mexico.

Reductions in the Labrador Sea Water formation and weakening of the subpolar gyre may be triggered by the expansion of Arctic sea ice and its melting in the Labrador Sea, a mechanism that has been widely invoked to explain the onset of North Atlantic cooling during the LIA (*6*, *9*, *10*). We posit that the associated weakening of the North Atlantic circulation, combined with reduced meridional salt transfer, could have amplified changes in the Labrador Sea and the subpolar gyre and thus reinforced the initial transient cooling driven by sea-ice-ocean feedbacks during the LIA (*6*, *9*, *10*) and other cold epochs of the C.E. (e.g., around 600 C.E. and 800 C.E). In contrast, slow advection of positive tropical SSS anomalies into the Labrador Sea and their release through mixing can help to weaken ocean stratification, promote deep water formation, strengthen the subpolar gyre and meridional oceanic transport, and eventually contribute to the mild climate conditions over Europe and North America [see, e.g., (*32*)].

In summary, the Caribbean SST/SSS records presented here provide evidence for pronounced changes in the northward transport of (sub)tropical salt linked with variability in the North Atlantic surface circulation during the C.E. These results underscore the ocean's critical role in climate variability of the historical past and have implications for understanding future climate change. However, because of limitations of existing sedimentary records (e.g., dating uncertainties and bioturbation), more data are needed to better constrain tropical-to-subpolar ocean interactions on centennial timescales.

MATERIALS AND METHODS

Materials

Giant box core M35003-6 (12°5.1′N, 61°14.7′W, 1299-m water depth) was recovered from the western flank of the Tobago Basin aboard the R/V Meteor in 1996. The core was taken by a large-sized trigger device that retrieves sediments with negligible compaction, and an undisturbed topmost surface (50 cm by 50 cm). The

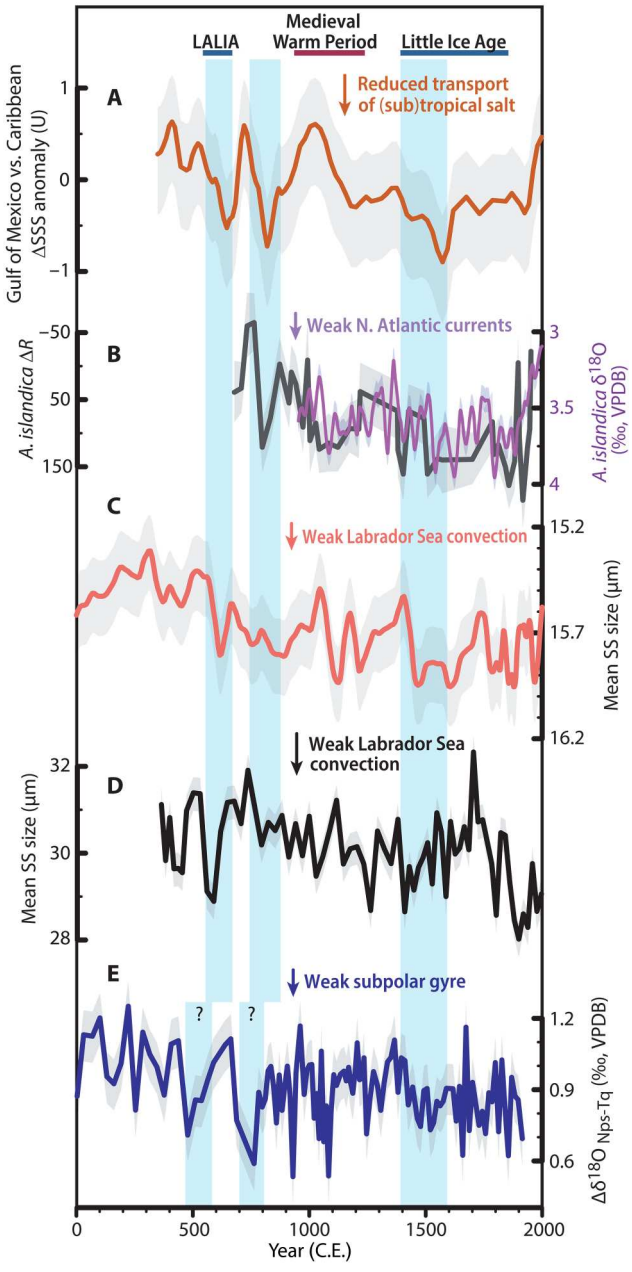

Fig. 6. Comparison of proxy records across the North Atlantic during the past 2000 years. (**A**) Difference between SSS anomalies (±1σ) in the Gulf of Mexico (*14*) and the southeastern Caribbean (this study). (**B**) Radiocarbon reservoir age offset [Δ*R*, gray, (*12*)] and a loess-filtered (5% smoothing span) record of $\delta^{18}O$ values [purple, (*13*)] in shells of the long-lived marine bivalve *A. islandica* from the North Icelandic shelf. (**C** and **D**) Mean sortable silt size (SS) records in core RAPiD-21-COM from the subpolar Northeastern Atlantic [loess-filtered, 5% smoothing span, (*10*)] and core KNR-178-48JPC from the western North Atlantic (*47*). (**E**) Difference in the $\delta^{18}O$ measurements of *N. pachyderma* (s) and *T. quinqueloba* in core RAPiD-35-COM from the Labrador Sea (*10*). For locations of sites, refer to Fig. 1B and table S1. Blue bars denote coherent cooling/salinification in the southeastern Caribbean and cooling/freshening in the Gulf of Mexico linked with the weakening of the North Atlantic surface circulation.

core (length of 45 cm) was continuously cut into 0.5-cm thick slices, and samples were then freeze-dried, washed over a 63-μm sieve, and the residues were dried at 40°C.

Stable isotope and Mg/Ca analyses

For stable oxygen and carbon isotope ($\delta^{18}O$ and $\delta^{13}C$) and Mg/Ca analyses about 60 specimens of *G. ruber* (white) sensu stricto were picked from the >150-μm fraction, cracked between glass plates, and then split for Mg/Ca and isotope measurements. $\delta^{18}O$ and $\delta^{13}C$ values in *G. ruber* (white) were measured using a Finnigan MAT 253 Plus mass spectrometer coupled to an automated carbonate preparation ("Kiel") device at Isotope Laboratory at Faculty of Geosciences, University of Bremen. For stable isotope measurements, a working standard was used, which has been calibrated against Vienna Pee Dee Belemnite (VPDB) by using the NBS 19 standard. The resulting $\delta^{18}O$ and $\delta^{13}C$ values are expressed in per mil relative to the VPDB standard notation (‰ VPDB). No significant outliers were found using PAST software (*48*). The long-term 1σ analytical uncertainty of the standard analyses was better than ±0.07‰ for oxygen and ±0.04‰ for carbon.

Trace element analysis was performed following the cleaning procedure described in (*49*), which is a slight modification of the originally proposed protocol (*50*) and consists of five water washes and two methanol washes, followed by two oxidation steps with 1% NaOH-buffered H_2O_2 and a weak acid leach with 0.001 M QD HNO_3. Afterward, samples were dissolved with 0.075 M QD HNO_3 and centrifuged for 10 min, transferred into test tubes, and diluted. Mg/Ca values were measured using a Perkin Elmer Optima 3300 R inductively coupled plasma optical emission spectrophotometer at MARUM, University of Bremen. There is no trend between Mn/Ca and Al/Ca to Mg/Ca, supporting the cleaning effectiveness and showing that Mg/Ca is not substantially affected by contamination or diagenesis. Mg/Ca values are expressed in millimoles per mole. One outlier has been identified and removed using PAST software (*48*). Instrumental precision was controlled using an external in-house (Mg/Ca = 2.92 mmol/mol) and ECRM 752-1 standards, measured after every 5th and 50th sample, respectively. The relative SD (1σ) was 0.014 mmol/mol (0.47%) for the external standard (n = 70) and 0.005 mmol/mol (0.12%) for ECRM 752-1 (n = 6). The average 1σ analytical precision was determined to be ±0.01 mmol/mol based on these standards. Replicate samples (n = 3) revealed an average 2σ SD of 0.11 mmol/mol.

SST and SSS reconstructions, uncertainties, and error propagation

Mg/Ca values in planktic foraminifera are controlled primarily by temperature (+6% per degree Celsius), but also salinity (ca. +4% per salinity unit), pH (−5 to −9% per 0.1 pH unit), and dissolution (*51*). The global pH effects on Mg/Ca and potentially on $\delta^{18}O$ were neglected because pH is expected to have changed only slightly over the past 1700 years (*52*). The local pH effects associated with the variable Orinoco discharge were considered minimal because of the lack of correlation between reconstructed SSS and runoff proxies (see Results; Fig. 2). Also, dissolution influence on Mg/Ca was neglected at our intermediate-depth (1299 m) site well above the critical 2500-m water depth below which substantial Mg^{2+} removal occurs (*53*). To account for the effects of salinity on the Mg/Ca data, we used a multivariate calibration for cultured *G.*

ruber (white) (*54*). The algorithm used for this purpose is integrated into the PSU Solver (*23*), a MATLAB code that uses the bootstrap Monte Carlo simulations to probabilistically constrain and quantify records of SST and seawater $\delta^{18}O$ ($\delta^{18}O_{sw}$, linearly related to SSS) from paired Mg/Ca-$\delta^{18}O$ data in foraminifera. Simultaneous solutions for SST and $\delta^{18}O_{sw}$ at each sample depth were obtained by inverting the following relationship equations (*54*–*56*), respectively

$$\ln(Mg/Ca) = 0.08 * SST + 0.06 * SSS - 2.8$$

$$SST = 16.5 - 4.8 * (\delta^{18}O_c - \delta^{18}O_{sw} + 0.27) \text{ (low light equation)}$$

$$\delta^{18}O_{sw} = 0.55 * SSS - 18.98$$

where SST is water mass temperature, SSS is salinity, $\delta^{18}O_c$ is the measured $\delta^{18}O$ of foraminiferal calcite, and $\delta^{18}O_{sw}$ is $\delta^{18}O$ of seawater. The 0.27‰ term is subtracted from the $\delta^{18}O_{sw}$ term to convert from the VPDB scale (calcite measurements) to the Vienna Standard Mean Ocean Water (seawater measurements) scale. For the conversion of $\delta^{18}O_{sw}$ into salinity units, we assumed that the regional $\delta^{18}O_{sw}$-SSS slope did not change over the past 1700 years.

PSU Solver was also used to quantify uncertainties of the reconstruction. Thus, at each sampling depth, we allowed Mg/Ca and $\delta^{18}O$ values to vary (n = 1000) between their associated combined analytical and sampling uncertainty to generate probability distributions around the measured value. The average 1σ (2σ) uncertainties are about ±0.5°C (0.8°C) for SST and ±0.3 U (0.6) for SSS. These errors include calibration errors, 2σ combined analytical and sampling uncertainty for Mg/Ca (±0.11 mmol/mol) and 2σ analytical uncertainty for $\delta^{18}O$ (±0.14‰). The age uncertainties were not included in the error propagation, but instead, three-point moving averages were used for interpretation.

Seasonality of foraminiferal SST/SSS

To accurately interpret foraminifera-based SST/SSS estimates, the seasonality of *G. ruber* (white) fluxes must be considered. *G. ruber* (white) occurs uniformly throughout the year in tropical environments, but its seasonal fluxes could vary at our site due to the variable influence of the Orinoco River, possibly biasing fossil assemblage composition toward the wet (summer/fall) or dry (winter) seasons. While river-borne nutrients enhance food availability for planktic foraminifera (*22*, *26*, *27*), images of chlorophyll concentration (https://oceancolor.gsfc.nasa.gov/l3/) show that the coring site in the southern Tobago Basin is influenced by nutrient-rich waters from the Orinoco and Amazon Rivers throughout the year, in contrast to regions characterized by high seasonal variability in planktic foraminifera production (*22*). Furthermore, freshwater plumes have been shown to negatively affect shallow-dwelling *G. ruber* (white) due to high turbidity, low light transmittance, and salt stress (*21*, *22*). Such inhibitory effects have been noted not only near but also far from the Orinoco, such as in the eastern Caribbean Basin (*21*) and offshore Lesser Antilles (*22*). Plankton studies in the Tobago Basin have been conducted only in spring (*21*, *22*) when the Orinoco discharge is low (*27*). Therefore, direct evidence of the effects of the freshwater/suspension plume on *G. ruber* (white) production during peak Orinoco runoff is lacking. Barium-to-calcium ratios in foraminiferal calcite suggest that Orinoco plume does not impede the growth of *G. ruber* (white) in the wet season at our location (*21*); these results, however, do not imply a bias toward the wet season.

Changepoint detection in the SSS record

BEAST [Bayesian Estimator of Abrupt Change, Seasonal Change, and Trend; (*24*)] was used to identify the changepoints and trends in the smoothed (three-point moving average) SSS reconstruction derived from the PSU Solver (see above). We applied the 'beast' function in the Rbeast package v0.9.7 in R 3.6.3, using default values and no periodic components defined in the time series. BEAST output (fig. S7) suggests that the SSS trend component has five change points (median number). These change points at 512 C.E. (with a summed probability of 0.30), 702 C.E. (0.72), 834 C.E. (0.70), 1537 C.E. (0.88), and 1670 C.E. (0.36) support the statistical significance of the SSS changes between 550 and 900 C.E. and an increase in surface salinity during the LIA.

Planktic foraminifera assemblages and lithic grains

Planktic foraminifera species and lithic grains were counted in the size fraction of >150 μm (figs. S2 and S3); a minimum of 600 specimens has been identified per sample (n = 90). Large specimens of *N. dutertrei* were counted together with smaller juvenile specimens referred to as *N. dutertrei*–*N. pachyderma* (dextral)-intergrades. The confidence limits (95%) of species proportions in foraminiferal assemblages were calculated after (*57*). To summarize patterns within the dataset, the PCA was performed using PAST software (*48*). PCA was carried out on species making out at least 3% of the assemblage (n = 10), which is statistically reliable (*57*). Bootstrapping was performed (n = 1000) to determine the 95% bootstrapped confidence intervals for the eigenvalues. The scree plot of the eigenvalues of PCs indicates that PC1, -2, and -3 (accounting for 75% of the total variance) are significant (figs. S4 and S5).

Supplementary Materials

This PDF file includes:
Supplementary Text
Figs. S1 to S7
Tables S1 to S4
References

Other Supplementary Material for this manuscript includes the following:
Data S1 and S2

REFERENCES AND NOTES

1. P. Braconnot, S. P. Harrison, M. Kageyama, P. J. Bartlein, V. Masson-Delmotte, A. Abe-Ouchi, B. Otto-Bliesner, Y. Zhao, Evaluation of climate models using palaeoclimatic data. *Nat. Clim. Change* **2**, 417–424 (2012).
2. U. Büntgen, V. S. Myglan, F. C. Ljungqvist, M. McCormick, N. Di Cosmo, M. Sigl, J. Jungclaus, S. Wagner, P. J. Krusic, J. Esper, J. O. Kaplan, M. A. C. de Vaan, J. Luterbacher, L. Wacker, W. Tegel, A. V. Kirdyanov, Cooling and societal change during the Late Antique Little Ice Age from 536 to around 660 AD. *Nat. Geosci.* **9**, 231–236 (2016).
3. V. Masson-Delmotte, M. Schulz, A. Abe-Ouchi, J. Beer, J. Ganopolski, J. F. González Rouco, E. Jansen, K. Lambeck, J. Luterbacher, T. Naish, T. Osborn, B. Otto-Bliesner, T. Quinn, R. Ramesh, M. Rojas, X. Shao, A. Timmermann, Information from paleoclimate archives. *Climate Change 2013: The Physical Science Basis. Contribution of Working Group I to the Fifth Assessment Report of the Intergovernmental Panel on Climate Change*. T. F. Stocker, D. Qin, G.-K. Plattner, M. Tignor, S. K. Allen, J. Doschung, A. Nauels, Y. Xia, V. Bex, and P. M. Midgley, Eds., (Cambridge Univ. Press, 2013), pp. 383–464.

4. M. E. Mann, Z. Zhang, S. Rutherford, R. S. Bradley, M. K. Hughes, D. Shindell, C. Ammann, G. Faluvegi, F. Ni, Global signatures and dynamical origins of the Little Ice Age and Medieval Climate Anomaly. *Science* **326**, 1256–1260 (2009).
5. R. Neukom, N. Steiger, J. J. Gómez-Navarro, J. Wang, J. P. Werner, No evidence for globally coherent warm and cold periods over the preindustrial Common Era. *Nature* **571**, 550–554 (2019).
6. P. Moffa-Sánchez, E. Moreno-Chamarro, D. J. Reynolds, P. Ortega, L. Cunningham, D. Swingedouw, J. Amrhein, J. Halfar, L. Jonkers, J. H. Jungclaus, K. Perner, A. Wanamaker, S. Yeager, Variability in the northern North Atlantic and Arctic Oceans across the last two millennia: A review. *Paleoceanogr. Paleoclimatol.* **34**, 1399–1436 (2019).
7. J. Slawinska, A. Robock, Impact of volcanic eruptions on decadal to centennial fluctuations of Arctic sea ice extent during the last millennium and on initiation of the little ice age. *J. Climate* **31**, 2145–2167 (2018).
8. P. Moffa-Sánchez, A. Born, I. R. Hall, D. J. R. Thornalley, S. Barker, Solar forcing of North Atlantic surface temperature and salinity over the past millennium. *Nat. Geosci.* **7**, 275–278 (2014).
9. F. Lehner, A. Born, C. C. Raible, T. F. Stocker, Amplified inception of European Little Ice Age by sea ice–ocean–atmosphere feedbacks. *J. Climate* **26**, 7586–7602 (2013).
10. P. Moffa-Sánchez, I. R. Hall, North Atlantic variability and its links to European climate over the last 3000 years. *Nat. Commun.* **8**, 1726 (2017).
11. D. C. Lund, J. Lynch-Stieglitz, W. B. Curry, Gulf Stream density structure and transport during the past millennium. *Nature* **444**, 601–604 (2006).
12. A. D. Wanamaker Jr., P. G. Butler, J. D. Scourse, J. Heinemeier, J. Eiríksson, K. L. Knudsen, C. A. Richardson, Surface changes in the North Atlantic Meridional Overturning Circulation during the last millennium. *Nat. Commun.* **3**, 899 (2012).
13. D. J. Reynolds, J. D. Scourse, P. R. Halloran, A. J. Nederbragt, A. D. Wanamaker, P. G. Butler, C. A. Richardson, J. Heinemeier, J. Eiríksson, K. L. Knudsen, I. R. Hall, Annually resolved North Atlantic marine climate over the last millennium. *Nat. Commun.* **7**, 13502 (2016).
14. K. Thirumalai, T. M. Quinn, Y. Okumura, J. N. Richey, J. W. Partin, R. Z. Poore, E. Moreno-Chamarro, Pronounced centennial-scale Atlantic Ocean climate variability correlated with Western Hemisphere hydroclimate. *Nat. Commun.* **9**, 392 (2018).
15. F. Lapointe, R. S. Bradley, P. Francus, N. L. Balascio, M. B. Abbott, J. Stoner, G. St-Onge, A. De Coninck, T. Labarre, Annually resolved Atlantic sea surface temperature variability over the past 2,900 y. *Proc. Natl. Acad. Sci. U.S.A.* **117**, 27171–27178 (2020).
16. J. Nyberg, B. A. Malmgren, A. Kuijpers, A. A. Winter, A centennial-scale variability of tropical North Atlantic surface hydrography during the late Holocene. *Palaeogeogr. Palaeoclimatol. Palaeoecol.* **183**, 25–41 (2002).
17. K. H. Kilbourne, M. A. Alexander, J. A. Nye, A low latitude paleoclimate perspective on Atlantic multidecadal variability. *J. Mar. Sys.* **133**, 4–13 (2014).
18. J. E. Tierney, N. J. Abram, K. J. Anchukaitis, M. N. Evans, C. Giry, K. H. Kilbourne, C. P. Saenger, H. C. Wu, J. Zinke, Tropical sea surface temperatures for the past four centuries reconstructed from coral archives. *Paleoceanography* **30**, 226–252 (2015).
19. J. B. Wurtzel, D. E. Black, R. C. Thunell, L. C. Peterson, E. J. Tappa, S. Rahman, Mechanisms of southern Caribbean SST variability over the last two millennia. *Geophys. Res. Lett.* **40**, 5954–5958 (2013).
20. A. Zhuravleva, M. Hüls, R. Tiedemann, H. A. Bauch, A 125-ka record of northern South American precipitation and the role of high-to-low latitude teleconnections. *Quat. Sci. Rev.* **270**, 107159 (2021).
21. A. Bahr, J. Schönfeld, J. Hoffmann, S. Voigt, R. Aurahs, M. Kucera, S. Flögel, A. Jentzen, A. Gerdes, Comparison of Ba/Ca and δO^{18}_{WATER} as freshwater proxies: A multi-species core-top study on planktonic foraminifera from the vicinity of the Orinoco River mouth. *Earth Planet. Sci. Lett.* **383**, 45–57 (2013).
22. B. Schmuker, R. Schiebel, Planktic foraminifers and hydrography of the eastern and northern Caribbean Sea. *Mar. Micropaleontol.* **46**, 387–403 (2002).
23. K. Thirumalai, T. M. Quinn, G. Marino, Constraining past seawater $\delta^{18}O$ and temperature records developed from foraminiferal geochemistry. *Paleoceanography* **31**, 1409–1422 (2016).
24. K. Zhao, M. A. Wulder, T. Hu, R. Bright, Q. Wu, H. Qin, Y. Li, E. Toman, B. Mallick, X. Zhang, M. Brown, Detecting change-point, trend, and seasonality in satellite time series data to track abrupt changes and nonlinear dynamics: A Bayesian ensemble algorithm. *Remote Sens. Environ.* **232**, 111181 (2019).
25. A. Mora, A. Laraque, P. Moreira-Turcq, J. A. Alfonso, Temporal variation and fluxes of dissolved and particulate organic carbon in the Apure, Caura and Orinoco rivers, Venezuela. *J. South. Am. Earth Sci.* **54**, 47–56 (2014).
26. F. E. Müller-Karger, C. R. McClain, T. R. Fisher, W. E. Esaias, R. Varela, Pigment distribution in the Caribbean sea: Observations from space. *Prog. Oceanogr.* **23**, 23–64 (1989).
27. R. López, J. M. López, J. Morell, J. E. Corredor, C. E. del Castillo, Influence of the Orinoco River on the primary production of eastern Caribbean surface waters. *J. Geophys. Res. Oceans* **118**, 4617–4632 (2013).
28. C. Wang, L. Zhang, S. K. Lee, Response of freshwater flux and sea surface salinity to variability of the Atlantic warm pool. *J. Climate* **26**, 1249–1267 (2013).
29. C. Y. Da-Allada, G. Alory, Y. du Penhoat, E. Kestenare, F. Durand, N. M. Hounkonnou, Seasonal mixed-layer salinity balance in the tropical Atlantic Ocean: Mean state and seasonal cycle. *J. Geophys. Res. Oceans* **118**, 332–345 (2013).
30. C. Wang, D. B. Enfield, S. K. Lee, C. W. Landsea, Influences of the Atlantic Warm Pool on Western Hemisphere summer rainfall and Atlantic hurricanes. *J. Climate* **19**, 3011–3028 (2006).
31. T. Bhattacharya, J. C. H. Chiang, W. Cheng, Ocean-atmosphere dynamics linked to 800–1050 CE drying in Mesoamerica. *Quat. Sci. Rev.* **169**, 263–277 (2019).
32. L. Zhang, C. Wang, S. K. Lee, Potential role of Atlantic Warm Pool-induced freshwater forcing in the Atlantic Meridional Overturning Circulation: Ocean–sea ice model simulations. *Climate Dynam.* **43**, 553–574 (2014).
33. J. H. Curtis, D. A. Hodell, M. Brenner, Climate variability on the Yucatan Peninsula (Mexico) during the past 3500 years, and implications for Maya cultural evolution. *Quatern. Res.* **46**, 37–47 (1996).
34. M. Medina-Elizalde, E. J. Rohling, Collapse of classic Maya civilization related to modest reduction in precipitation. *Science* **335**, 956–959 (2012).
35. D. J. Kennett, S. F. M. Breitenbach, V. V. Aquino, Y. Asmerom, J. Awe, J. U. L. Baldini, P. Bartlein, B. J. Culleton, C. Ebert, C. Jazwa, M. J. Macri, N. Marwan, V. Polyak, K. M. Prufer, H. E. Ridley, H. Sodemann, B. Winterhalder, G. H. Haug, Development and disintegration of Maya political systems in response to climate change. *Science* **338**, 788–791 (2012).
36. M. J. Burn, S. E. Palmer, Solar forcing of Caribbean drought events during the last millennium. *J. Quat. Sci.* **29**, 827–836 (2014).
37. A. Winter, T. Miller, Y. Kushnir, A. Sinha, A. Timmermann, M. R. Jury, C. Gallup, H. Cheng, R. L. Edwards, Evidence for 800 years of North Atlantic multi-decadal variability from a Puerto Rican speleothem. *Earth Planet. Sci. Lett.* **308**, 23–28 (2011).
38. C. Fensterer, D. Scholz, D. Hoffmann, C. Spötl, J. M. Pajón, A. Mangini, Cuban stalagmite suggests relationship between Caribbean precipitation and the Atlantic Multidecadal Oscillation during the past 1.3 ka. *Holocene* **22**, 1405–1412 (2012).
39. G. H. Haug, K. A. Hughen, D. M. Sigman, L. C. Peterson, U. Röhl, Southward migration of the intertropical convergence zone through the Holocene. *Science* **293**, 1304–1308 (2001).
40. D. B. Enfield, A. M. Mestas-Nuñez, P. J. Trimble, The Atlantic multidecadal oscillation and its relation to rainfall and river flows in the continental U.S. *Geophys. Res. Lett.* **28**, 2077–2080 (2001).
41. A. R. Friedman, G. Reverdin, M. Khodri, G. Gastineau, A new record of Atlantic sea surface salinity from 1896 to 2013 reveals the signatures of climate variability and long-term trends. *Geophys. Res. Lett.* **44**, 1866–1876 (2017).
42. D. L. R. Hodson, P.-A. Bretonnière, C. Cassou, P. Davini, N. P. Klingaman, K. Lohmann, J. Lopez-Parages, M. Martín-Rey, M.-P. Moine, P.-A. Monerie, D. A. Putrasahan, C. D. Roberts, J. Robson, Y. Ruprich-Robert, E. Sanchez-Gomez, J. Seddon, R. Senan, Coupled climate response to Atlantic multidecadal variability in a multi-model multi-resolution ensemble. *Climate Dynam.* **59**, 805–836 (2022).
43. D. Zhang, R. Msadek, M. J. McPhaden, T. Delworth, Multidecadal variability of the North Brazil Current and its connection to the Atlantic meridional overturning circulation. *J. Geophys. Res. Oceans* **116**, C04012 (2011).
44. P. del Monte-Luna, H. Villalobos, F. Arreguín-Sánchez, Variability of sea surface temperature in the southwestern Gulf of Mexico. *Cont. Shelf Res.* **102**, 73–79 (2015).
45. W. E. Johns, T. L. Townsend, D. M. Fratantoni, W. Wilson, On the Atlantic inflow to the Caribbean Sea. *Deep Sea Res. I Oceanogr. Res. Pap.* **49**, 211–243 (2002).
46. E. Moreno-Chamarro, D. Zanchettin, K. Lohmann, J. H. Jungclaus, An abrupt weakening of the subpolar gyre as trigger of Little Ice Age-type episodes. *Clim. Dynam.* **48**, 727–744 (2017).
47. D. J. R. Thornalley, D. W. Oppo, P. Ortega, J. I. Robson, C. M. Brierley, R. Davis, I. R. Hall, P. Moffa-Sanchez, N. L. Rose, P. T. Spooner, I. Yashayaev, L. D. Keigwin, Anomalously weak Labrador Sea convection and Atlantic overturning during the past 150 years. *Nature* **556**, 227–230 (2018).
48. Ø. Hammer, D. A. T. Harper, P. D. Ryan, PAST: Paleontological statistics software package for education and data analysis. *Palaeontol. Electron.* **4**, 9 (2001).
49. M. Mohtadi, M. Prange, D. W. Oppo, R. De Pol-Holz, U. Merkel, X. Zhang, S. Steinke, A. Lückge, North Atlantic forcing of tropical Indian Ocean climate. *Nature* **509**, 76–80 (2014).
50. S. Barker, M. Greaves, H. Elderfield, A study of cleaning procedures used for foraminiferal Mg/Ca paleothermometry. *Geochem. Geophys. Geosyst.* **4**, 8407 (2003).
51. W. R. Gray, S. Weldeab, D. W. Lea, Y. Rosenthal, N. Gruber, B. Donner, G. Fischer, The effects of temperature, salinity, and the carbonate system on Mg/Ca in Globigerinoides ruber (white): A global sediment trap calibration. *Earth Planet. Sci. Lett.* **482**, 607–620 (2018).

52. W. R. Gray, D. Evans, Nonthermal influences on Mg/Ca in planktonic foraminifera: A review of culture studies and application to the last glacial maximum. *Paleoceanogr. Paleoclimatol.* **34**, 306–315 (2019).
53. M. Regenberg, D. Nürnberg, S. Steph, J. Groeneveld, D. Garbe-Schönberg, R. Tiedemann, W.-C. Dullo, Assessing the effect of dissolution on planktonic foraminiferal Mg/Ca ratios: Evidence from Caribbean core tops. *Geochem. Geophys. Geosyst.* **7**, 10.1029/2005GC001019, (2006).
54. B. Kısakürek, A. Eisenhauer, F. Böhm, D. Garbe-Schönberg, J. Erez, Controls on shell Mg/Ca and Sr/Ca in cultured planktonic foraminiferan, Globigerinoides ruber (white). *Earth Planet. Sci. Lett.* **273**, 260–269 (2008).
55. B. E. Bemis, H. J. Spero, J. Bijma, D. W. Lea, Reevaluation of the oxygen isotopic composition of planktonic foraminifera: Experimental results and revised paleotemperature equations. *Paleoceanography* **13**, 150–160 (1998).
56. A. N. LeGrande, G. A. Schmidt, Global gridded data set of the oxygen isotopic composition in seawater. *Geophys. Res. Lett.* **33**, L12604 (2006).
57. F. Fatela, R. Taborda, Confidence limits of species proportions in microfossil assemblages. *Mar. Micropaleontol.* **45**, 169–174 (2002).
58. H. Zuo, M. A. Balmaseda, S. Tietsche, K. Mogensen, M. Mayer, The ECMWF operational ensemble reanalysis–analysis system for ocean and sea ice: A description of the system and assessment. *Ocean Sci.* **15**, 779–808 (2019).
59. T. P. Boyer, J. I. Antonov, O. K. Baranova, H. E. Garcia, D. R. Johnson, A. V. Mishonov, T. D. O'Brien, D. Seidov, I. Smolyar, M. M. Zweng, C. R. Paver, World ocean database 2013 (2013).
60. R. Schlitzer, Ocean Data View; https://odv.awi.de (2018).
61. J. N. Richey, K. Thirumalai, D. Khider, C. E. Reynolds, J. W. Partin, T. M. Quinn, Considerations for Globigerinoides ruber (white and pink) paleoceanography: Comprehensive insights from a long-running sediment trap. *Paleoceanogr. Paleoclimatol.* **34**, 353–373 (2019).
62. T. J. Heaton, P. Köhler, M. Butzin, E. Bard, R. W. Reimer, W. E. Austin, C. B. Ramsey, P. M. Grootes, K. A. Hughen, B. Kromer, P. J. Reimer, J. Adkins, A. Burke, M. S. Cook, J. Olsen, L. C. Skinner, Marine20—The marine radiocarbon age calibration curve (0–55,000 cal BP). *Radiocarbon* **62**, 779–820 (2020).
63. R. J. DiNapoli, S. M. Fitzpatrick, M. F. Napolitano, T. C. Rick, J. H. Stone, N. P. Jew, Marine reservoir corrections for the Caribbean demonstrate high intra- and inter-island variability in local reservoir offsets. *Quat. Geochronol.* **61**, 101126 (2021).
64. M. Blaauw, J. A. Christen, Flexible paleoclimate age-depth models using an autoregressive gamma process. *Bayesian Anal.* **6**, 457–474 (2011).
65. T. P. Guilderson, J. E. Cole, J. R. Southon, Pre-bomb Δ14C variability and the suess effect in cariaco basin surface waters as recorded in hermatypic corals. *Radiocarbon* **47**, 57–65 (2005).
66. A. J. Wagner, T. P. Guilderson, N. C. Slowey, J. E. Cole, Pre-bomb surface water radiocarbon of the Gulf of Mexico and Caribbean as recorded in hermatypic corals. *Radiocarbon* **51**, 947–954 (2009).
67. G. Rodriguez-Vera, R. Romero-Centeno, C. L. Castro, V. M. Castro, Coupled interannual variability of wind and sea surface temperature in the Caribbean sea and the Gulf of Mexico. *J. Climate* **32**, 4263–4280 (2019).
68. K. M. Yeager, P. H. Santschi, G. T. Rowe, Sediment accumulation and radionuclide inventories (239,240Pu, 210Pb and 234Th) in the northern Gulf of Mexico, as influenced by organic matter and macrofaunal density. *Mar. Chem.* **91**, 1–14 (2004).
69. M. H. Trauth, M. Sarnthein, M. Arnold, Bioturbational mixing depth and carbon flux at the seafloor. *Paleoceanography* **12**, 517–526 (1997).
70. M. Hüls, R. Zahn, Millennial-scale sea surface temperature variability in the western tropical North Atlantic from planktonic foraminiferal census counts. *Paleoceanography* **15**, 659–678 (2000).
71. S. Steph, M. Regenberg, R. Tiedemann, S. Mulitza, D. Nürnberg, Stable isotopes of planktonic foraminifera from tropical Atlantic/Caribbean core-tops: Implications for reconstructing upper ocean stratification. *Mar. Micropaleontol.* **71**, 1–19 (2009).

Acknowledgments: We are grateful to M. Hollstein, V. Rodehutscord, V. Floren, B. Meyer-Schack, M. Steinkamp, H. Kuhnert, S. Pape, and M. Kölling for laboratory assistance. **Funding:** This work was supported by DFG grants BA 1367/12-1 to H.A.B. and A.Z., the Cluster of Excellence "The Ocean Floor—Earth's Uncharted Interface to M.M., and the OFI Postdoctoral Fellowship Program (award number 39274) to A.Z. **Author contributions:** A.Z. and H.A.B. designed the study. M.M. measured Mg/Ca and $\delta^{18}O$ values in planktic foraminifera. A.Z. wrote the manuscript. H.A.B., M.M., K.F., and M.K. commented on the manuscript. Conceptualization: A.Z. Methodology: M.M. Investigation: A.Z. Visualization: A.Z. Writing—review and editing: A.Z., H.A.B., M.M., K.F., and M.K. **Competing interests:** The authors declare that they have no competing interests. **Data and materials availability:** All data needed to evaluate the conclusions in the paper are present in the paper, the Supplementary Materials, and at doi:10.1594/PANGAEA.962235. There are no restrictions associated with the use of these data.

Submitted 13 December 2022
Accepted 5 October 2023
Published 3 November 2023
10.1126/sciadv.adg2639